Evaluation of Tropical Cyclone Center Identification Methods in Numerical Models

LEON T. NGUYEN, JOHN MOLINARI, AND DIANA THOMAS

Department of Atmospheric and Environmental Sciences, University at Albany, State University of New York, Albany, New York

(Manuscript received 31 January 2014, in final form 11 June 2014)

ABSTRACT

Identifying the center of a tropical cyclone in a high-resolution model simulation has a number of operational and research applications, including constructing a track, calculating azimuthal means and perturbations, and diagnosing vortex tilt. This study evaluated several tropical cyclone center identification methods in a high-resolution Weather Research and Forecasting (WRF) Model simulation of a sheared, intensifying, asymmetric tropical cyclone. The simulated tropical cyclone (TC) contained downshear convective cells and a mesovortex embedded in a broader TC vortex, complicating the identification of the TC vortex center. It is shown that unlike other methods, the pressure centroid method consistently 1) placed the TC center within the region of weak storm-relative wind, 2) produced a smooth track, 3) yielded a vortex tilt that varied smoothly in magnitude and direction, and 4) was insensitive to changes in horizontal grid resolution. Based on these results, the authors recommend using the pressure centroid to define the TC center in high-resolution numerical models.

The pressure centroid was calculated within a circular region representing the size of the TC inner core. To determine this area, the authors propose normalizing by the innermost radius at which the azimuthally averaged storm-relative tangential wind at 2-km height equals 80% of the maximum (R_{80}) at 2-km height. Although compositing studies have often normalized by the radius of maximum wind (RMW), R_{80} proved less sensitive to slight changes in flat tangential wind profiles. This enables R_{80} to be used as a normalization technique not only with intense TCs having peaked tangential wind profiles, but also with weaker TCs having flatter tangential wind profiles.

1. Introduction

The tropical cyclone (TC) is characterized by a region of swirling winds on the order of several hundred to several thousand kilometers across. An accurate identification of the TC center has a number of applications beyond constructing the storm track. Transforming the TC domain into cylindrical coordinates provides a useful framework for studying TC structure and dynamics, but depends critically on a physically reasonable TC center position. The radial and tangential components of the wind field, azimuthal wavenumber decomposition, and radial gradients of physical variables all exhibit sensitivity to the location of the TC center, particularly toward smaller radii. For example, Willoughby (1992) showed that erroneous placement of the TC center in an axisymmetric wind field resulted in an apparent wavenumber-1 streamfunction asymmetry. This sensitivity can also have an impact on the radial advection and flux terms found in various budget calculations, including the tangential momentum and potential temperature budgets of tropical cyclones (e.g., Montgomery et al. 2006). Additionally, determining vortex tilt depends on a reliable estimate of the TC center at multiple vertical levels.

Several methods of identifying the center of a tropical cyclone have been used in observational and modeling studies. Using aircraft in situ data, Willoughby and Chelmow (1982) identified the TC center as the point that maximized the ''circulating flux'' within 50 s of the aircraft's closest center approach. Studies using single-Doppler (e.g., Lee and Marks 2000) and airborne dual-Doppler radar (e.g., Reasor et al. 2013) data defined the TC center as the location that maximized the tangential wind within an annulus centered on the radius of maximum wind (RMW). Some modeling studies have used the centroid of potential vorticity (e.g., Reasor and

Corresponding author address: Leon T. Nguyen, Department of Atmospheric and Environmental Sciences, University at Albany/SUNY, ES 325, 1400 Washington Ave., Albany, NY 12222.
E-mail: lnguyen@albany.edu

DOI: 10.1175/MWR-D-14-00044.1

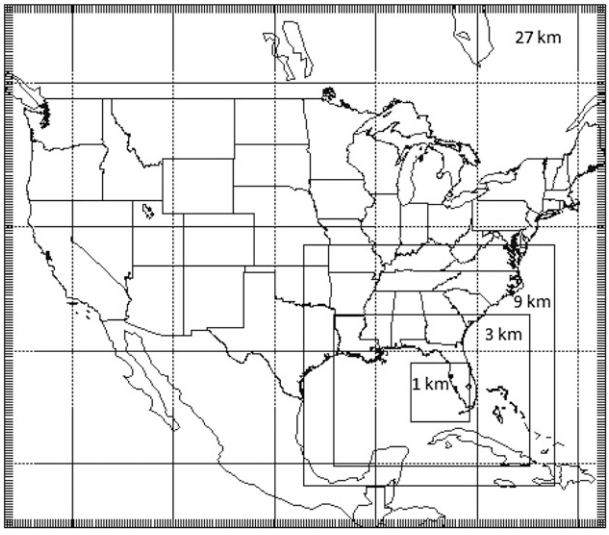

FIG. 1. Setup of the four nested domains used in the WRF simulation.

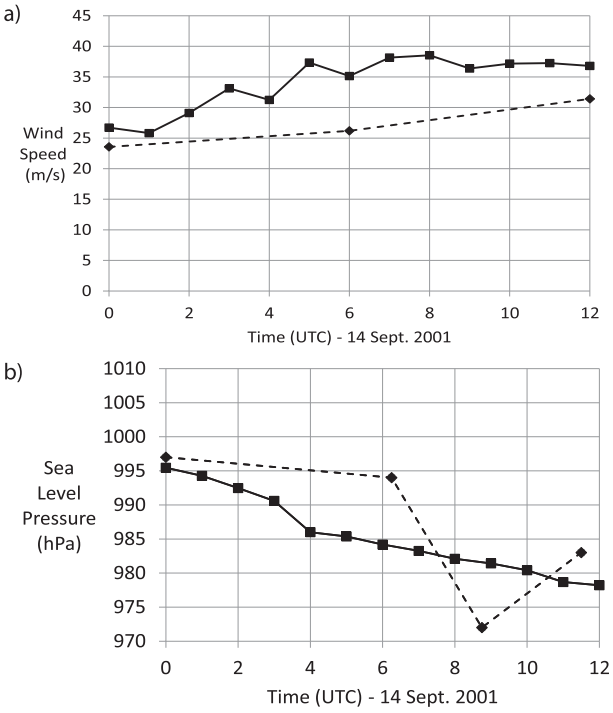

FIG. 2. (a) Maximum 10-m wind speed from the WRF simulation (solid line) and from NHC best track (dotted line). (b) Minimum sea level pressure from the WRF simulation (solid line) and from aircraft reconnaissance (dotted line).

Montgomery 2001) or relative vorticity (e.g., Riemer et al. 2010) within a box or circle of predetermined size. Modeling studies by Braun (2002) and Braun et al. (2006) defined the TC center as the location that minimized the azimuthal variance of the pressure field at all radii between the center and the outer portion of the eyewall. Cavallo et al. (2013) defined the TC center in a model as the location that maximized the 800-hPa circulation over a circle of 150-km radius. To our knowledge, the efficacy of these center identification methods has not yet been assessed and compared in any published work, thus motivating the current study.

Tropical Storm Gabrielle (2001) was an asymmetric, sheared tropical cyclone that underwent a period of short-term rapid intensification, with the minimum sea level pressure dropping 22 hPa in 2.5 h. Further details regarding the life cycle and the short-term rapid intensification were discussed by Molinari et al. (2006) and Molinari and Vollaro (2010). A high-resolution model simulation of this short-term rapid intensification was performed. A strong mesovortex and other convective asymmetries developed early in the simulation. The simulated tropical cyclone became more axisymmetric later in the simulation. This evolution provided a challenging case to assess and compare several tropical cyclone center identification methods.

2. Model setup

The Weather Research and Forecasting (WRF) Model version 3.2 (Skamarock et al. 2008) was used to simulate the rapid intensification period of Gabrielle's life cycle. The simulation utilized four nested domains of 27-, 9-, 3-, and 1-km horizontal resolution. Figure 1 shows the setup of the four domains. The 27- and 9-km domains were initialized at 1200 UTC 13 September, the 3-km domain was initialized at 1800 UTC 13 September, and the 1-km domain was initialized at 0000 UTC 14 September. The 1-km domain ran until 1500 UTC 14 September, while the remaining three domains ran until 0000 UTC 15 September. The National Centers for Environmental Prediction (NCEP) Global Forecast System (GFS) Final (FNL) operational global analyses were used for initial conditions and boundary conditions.

The model physics parameterizations used were as follows: The Kain–Fritsch cumulus parameterization on the 27- and 9-km domains (Kain and Fritsch 1993), the WRF single-moment 6-class microphysics scheme (WSM6; Hong and Lim 2006), the Dudhia shortwave radiation (Dudhia 1989) and the Rapid Radiative Transfer Model (RRTM) longwave radiation (Mlawer et al. 1997) schemes, and the Yonsei University planetary boundary layer scheme (Noh et al. 2003).

3. Evolution of the simulated tropical cyclone

Figure 2 shows the observed and simulated intensity evolution of the tropical cyclone between 0000 and 1200 UTC 14 September. The simulated maximum 10-m wind speed increased from 26 to 38 m s^{-1}, which compared

well with the observed wind speed from National Hurricane Center (NHC) best track (Fig. 2a). The simulated minimum sea level pressure fell from 995 to 978 hPa during the 12-h period, with the maximum 1-h pressure fall of 4.6 hPa occurring between 0300 and 0400 UTC (Fig. 2b). Although the magnitude of the extreme deepening rate observed in nature (22 hPa in 2.5 h) was not reproduced, the simulation intensified the TC amid strong ambient vertical wind shear. The 850–200-hPa vertical wind shear in the simulation, averaged within 500-km radius of the TC center, was from the west-southwest and increased from 9.4 m s^{-1} at 0000 UTC to 14.1 m s^{-1} at 1200 UTC. This compared well with the shear derived from European Centre for Medium-Range Weather Forecasts (ECMWF) gridded analysis by Molinari et al. (2006).

Figure 3 shows the evolution of sea level pressure and simulated reflectivity at 1-km height during the 0200–0500 UTC 14 September period. Of particular interest was a small-scale vortex (hereafter mesovortex) that developed at 0200 UTC (Fig. 3a) and revolved counterclockwise within the TC circulation over the next several hours (Fig. 3c) before beginning to coalesce with the TC circulation (Fig. 3d). During the 0600–1200 UTC time period (not shown), the TC became more axisymmetric. The formation of this mesovortex and its role in the intensification of the simulated tropical cyclone within strongly sheared environmental flow will be assessed in a forthcoming paper. Because the tropical cyclone in this simulation evolved from an asymmetric tropical storm with a strong mesovortex to a minimal hurricane with a more axisymmetric structure, this enabled TC center identification methods to be assessed for different types of TC structure.

4. Description of tropical cyclone center identification methods

Four methods will be discussed in this manuscript: the potential vorticity (PV) centroid, the maximum tangential wind, the maximum circulation, and the pressure centroid method. These methods can be applied to any vertical level in the atmosphere. The PV centroid was calculated as follows. First, the location of the minimum pressure on a constant height surface was used as the first guess, and the PV centroid was calculated within a circle of radius R around the first guess:

$$\bar{x} = \frac{\sum_{r=0}^{r=R} x_i \mathrm{PV}_i}{\sum_{r=0}^{r=R} \mathrm{PV}_i} \quad \text{and} \quad \bar{y} = \frac{\sum_{r=0}^{r=R} y_i \mathrm{PV}_i}{\sum_{r=0}^{r=R} \mathrm{PV}_i}, \tag{1}$$

where $\bar{x}$ and $\bar{y}$ represent the longitude and latitude, respectively, of the TC center; R represents the outer radius of the TC inner core; x_i and y_i are the grid points within the circle containing positive PV following Riemer et al. (2010); and PV_i represents the PV at those grid points. The resulting latitude and longitude were then used as the "new guess," and the procedure above was repeated until settling onto a single location. The PV centroid including both positive and negative PV was also tested and will be briefly discussed.

The maximum tangential wind method was performed by first subtracting the 6-hourly TC motion from the total wind field to yield a storm-relative wind. Then, all grid points within a 150-km radius of the pressure minimum were considered as potential TC centers. Radial profiles of azimuthally averaged tangential wind were calculated using each of these grid points as the TC center. The grid point that maximized the azimuthally averaged tangential wind within a 16-km-wide annulus centered on the radius of maximum wind was identified as the TC center following Reasor et al. (2013).

The maximum circulation method was performed as follows. Invoking Stokes's theorem, the circulation about a closed loop divided by the area enclosed equals the average normal component of vorticity within the area enclosed. Thus, the maximum circulation method identified the grid point that maximized the average vertical vorticity within a circle of 100-km radius as the TC center.

The pressure centroid on a constant height surface was calculated as follows. First, as in the PV centroid, the minimum pressure location was used as a first guess, and the pressure centroid was calculated over a circle of radius R:

$$\bar{x} = \frac{\sum_{r=0}^{r=R} x_i P_i'}{\sum_{r=0}^{r=R} P_i'} \quad \text{and} \quad \bar{y} = \frac{\sum_{r=0}^{r=R} y_i P_i'}{\sum_{r=0}^{r=R} P_i'}, \tag{2}$$

$$P_i' = P_{\mathrm{env}} - P_i, \tag{3}$$

where P_i' represents the pressure deficit, calculated by subtracting the pressure at each grid point from the environmental pressure averaged along the 500-km radius. Then, as in the PV centroid method, the resulting latitude and longitude were used as the next guess, and the procedure above was repeated until settling onto a single location. The minimization of azimuthal variance method used by Braun (2002) was also tested and yielded similar results to the pressure centroid method, but the pressure centroid method was preferred here because the computational time was about an order of magnitude less. Geopotential height can be substituted for pressure if one wishes to calculate the center on a constant pressure surface.

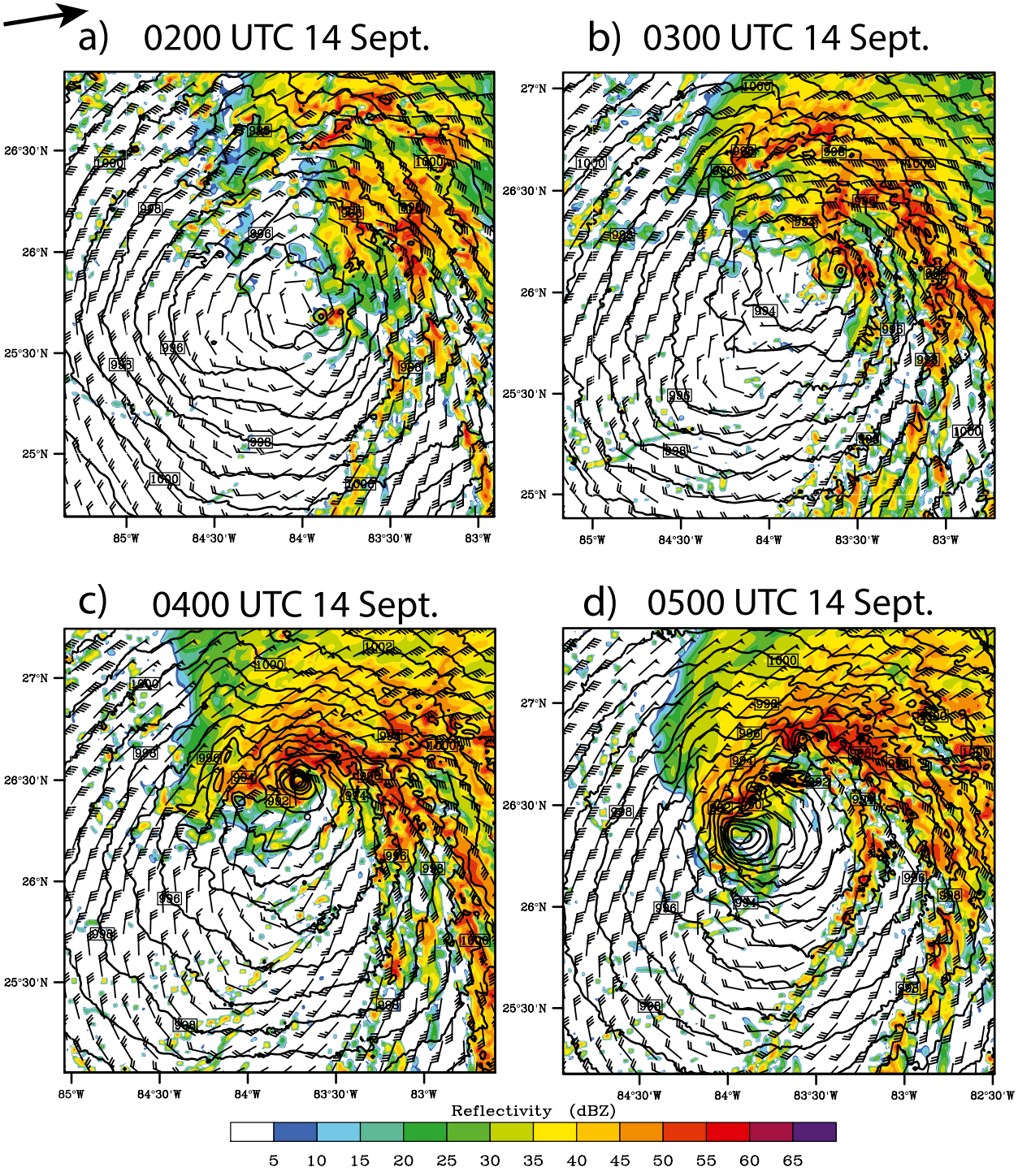

FIG. 3. Simulated reflectivity (shaded every 5 dBZ) at 1-km height, sea level pressure (contoured every 1 hPa), and 10-m winds. (top left) The approximate shear direction is shown.

5. Comparing the performance of center identification methods

The performance of the center identification methods was assessed based on four criteria. First, the TC center should be located within the region of weak storm-relative wind that is surrounded by strong cyclonic flow. If the method places the TC center within the region of strong cyclonic flow, it is not performing well. Second, as

proposed by Murillo et al. (2011), the motion of the TC center should be smooth over time and should not abruptly change speed and/or direction on an hourly time scale. Abrupt changes in TC motion on such a short time scale are much more likely to reflect erroneous and/or inconsistent identification of the TC center than a true shift in the motion of the TC. Trochoidal oscillations in the tracks of TCs have been seen both in observations (e.g., Jordan 1966; Griffin et al. 1992) and in model simulations (e.g., Liu et al. 1999), but these relatively smooth oscillations contrast with the abrupt "jumps" in the TC center position that will be shown and discussed below. The TC center reformations have also been observed (e.g., Molinari et al. 2006), but these events are typically comprised of a single discrete jump (instead of several) to the new center that forms near downshear convection. Third, the vortex tilt should vary smoothly in magnitude and direction throughout the depth of the vortex. Abrupt changes in the magnitude and/or direction of vortex tilt between adjacent vertical layers are inconsistent with a vortex that is vertically coherent, and thus are more likely to be a result of inconsistencies in identifying the TC center. Last, simply changing the horizontal resolution of the data should not change the analyzed TC center location significantly. Such a change would indicate sensitivity of the method to the horizontal resolution, which would limit the applicability of the method to simulations of other resolutions.

For this section, the potential vorticity centroid, pressure centroid, and maximum circulation methods were all calculated using a radius of 100 km to facilitate comparison.

a. *Center locations within the tropical cyclone wind field*

Figure 4 shows a comparison of four center identification methods at two vertical levels (2- and 8-km height) at three different times (0200, 0400, and 0600 UTC 14 September). The differences between the four methods were more pronounced early in the simulation, when the tropical cyclone was weaker and more asymmetric. As the simulated TC intensified and became more axisymmetric (particularly after 0600 UTC, not shown), the four methods increasingly agreed with each other.

At the 2-km level and to a lesser extent the 8-km level, the PV centroid was embedded in storm-relative winds of greater than 10 m s^{-1} and was persistently to the east-northeast of the region of weakest storm-relative winds. This was due to the numerous small-scale PV maxima generated by downshear convection that drew the PV centroid to that quadrant. The maximum circulation method also performed poorly and inconsistently, particularly at 2-km height. At 0200 UTC 14 September, the 2-km maximum circulation center was located on the western flank of the region of weak storm-relative winds. Two hours later, the 2-km maximum circulation center shifted to the southern flank, and by 0600 UTC, it was displaced more than 50 km to the east-southeast of the other center identification methods. The eastward displacement of the maximum circulation center persisted through the rest of the simulation (not shown). The maximum tangential wind method performed better than the previous two methods, although the 2-km center appeared to be too far to the west at 0200 UTC and the 8-km center appeared to be too far to the northeast at 0200 UTC. At 0400 UTC, much like the maximum circulation center, the 2-km maximum tangential wind center was displaced slightly too far to the south-southwest. The pressure centroid appeared to be the most effective at placing the center within the region of weak storm-relative winds of under 10 m s^{-1}. The 2-km pressure centroid did not follow the mesovortex; instead the mesovortex revolved around the pressure centroid, consistent with the physical interpretation that the mesovortex was feature embedded within, but distinct from the tropical cyclone vortex.

b. *Tracks*

Figure 5 shows the track of the tropical cyclone center at 2-km height from 0000 to 0600 UTC 14 September using the four aforementioned center identification methods as well as the location of the pressure minimum. The TC moved generally from southwest to northeast during this time period. Between 0000 and 0100 UTC, the PV centroid tracked toward the southeast, but then abruptly turned toward the northeast between 0100 and 0200 UTC. The maximum tangential wind center drifted slowly toward the west between 0000 and 0300 UTC, and then moved quickly toward the east-northeast over the 0300–0500 UTC period before moving toward the north-northwest by 0600 UTC. The maximum circulation center actually moved toward the southwest during the 0000–0100 UTC period before resuming a general east-northeast motion until 0600 UTC. The motion of the pressure minimum was also quite erratic. The pressure minimum moved toward the north-northeast during the 0000–0100 UTC period before abruptly moving south between 0100 and 0200 UTC. From 0200 to 0500 UTC, the pressure minimum tracked the mesovortex and made a cyclonic loop. These abrupt changes in track direction and/or speed over short time scales likely reflect inconsistencies in the identification of the TC center instead of any change in the motion of the TC. In contrast to the other center identification methods, the pressure centroid track was quite smooth.

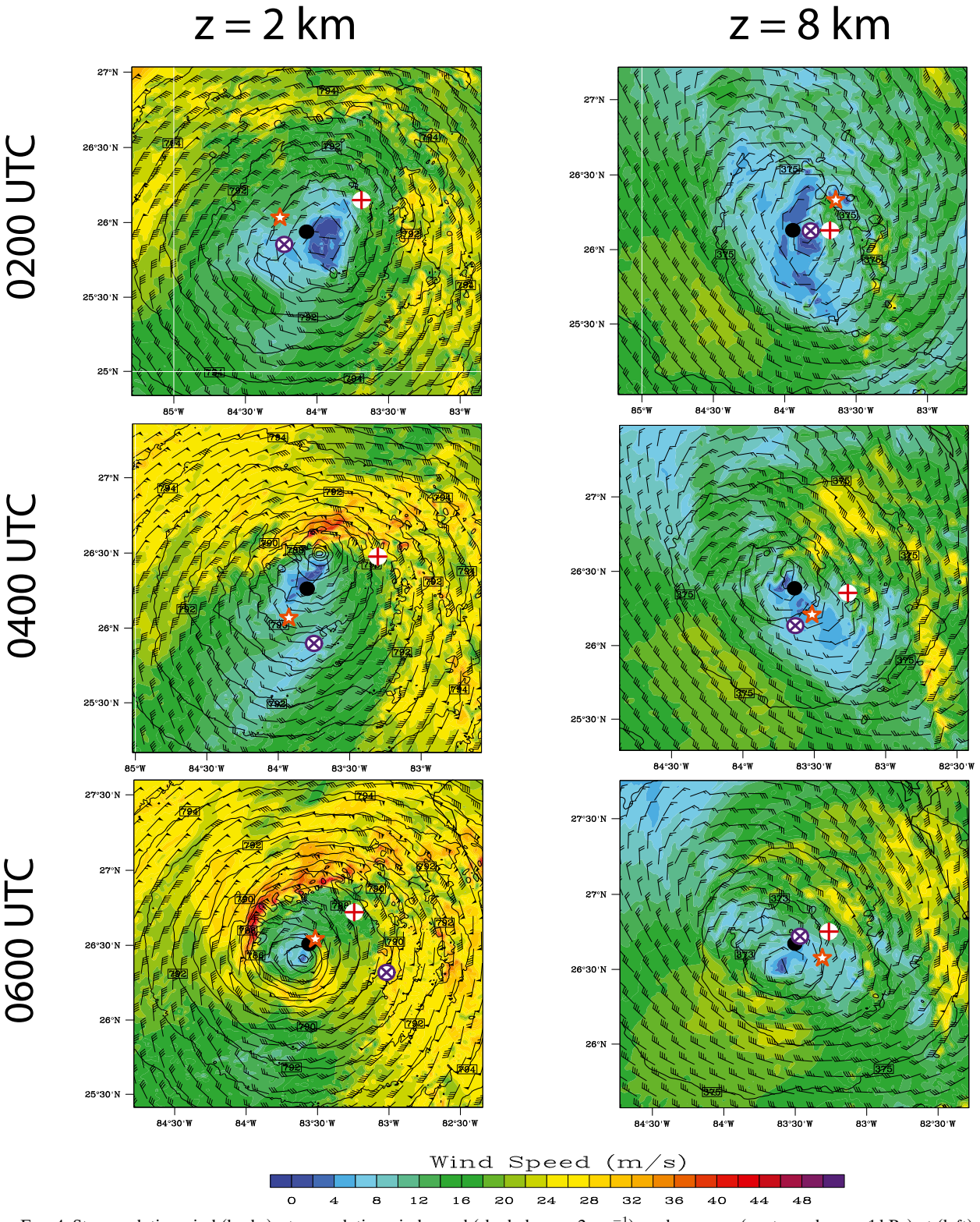

FIG. 4. Storm-relative wind (barbs), storm-relative wind speed (shaded every 2 m s^{-1}), and pressure (contoured every 1 hPa) at (left) 2-km height and (right) 8-km height. The tropical cyclone center diagnosed using the 0–100-km pressure centroid (black filled circle), 0–100-km potential vorticity centroid (red plus sign), the maximum tangential wind (orange star), and the maximum 100-km circulation (purple circled "×") methods are shown.

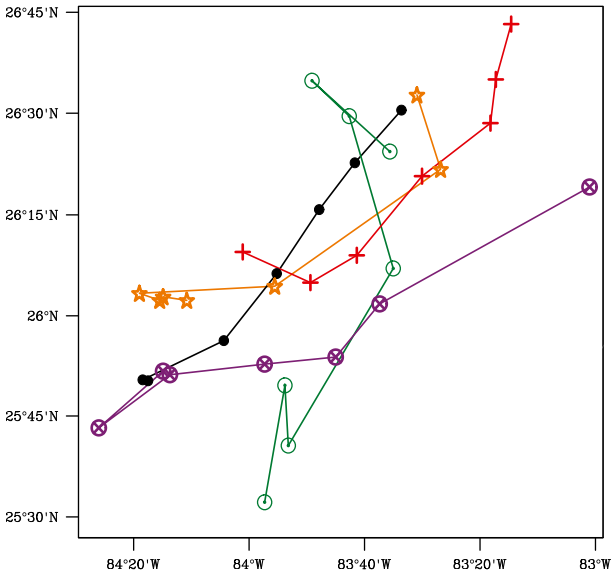

FIG. 5. Track of the tropical cyclone center at 2-km height in the WRF simulation from 0000 to 0600 UTC 14 Sep using the pressure centroid (black filled circle), PV centroid (red plus sign), maximum tangential wind (orange star), maximum circulation (purple circled "×"), and minimum pressure (green open circle) methods. The symbols represent the TC center at each hour.

Between 0000 and 0100 UTC, the pressure centroid was nearly stationary, but between 0100 and 0600 UTC, the pressure centroid moves consistently toward the northeast.

c. *Vortex tilt profiles*

Figure 6 shows the vortex tilt profiles using the centers identified with the pressure centroid, maximum tangential wind, potential vorticity centroid, and maximum circulation methods at 0200, 0400, and 0600 UTC 14 September. The PV centroid method did not yield a realistic vertical structure of vortex tilt (Figs. 6d–f). At all times shown, the vortex tilt magnitude was much larger in the 0–2-km layer than in any subsequent layer, which was not only unrealistic but also contrasted with the other three methods. The maximum circulation method yielded a very erratic vortex tilt, particularly at 0400 and 0600 UTC (Figs. 6k,l). The maximum tangential wind method yielded a somewhat more realistic vortex tilt profile. One exception was at 0400 UTC (Fig. 6h), when the vortex was tilted toward the north-northwest in the 0–2-km layer, was nearly upright in the 2–4-km layer, and then was tilted nearly 40 km toward the northeast in the 4–6-km layer. Because we suspect the TC vortex to be a coherent and continuous structure with height, the irregular, zigzag nature of the PV centroid, maximum tangential wind, and maximum circulation vortex tilt profiles is unrealistic and unphysical.

In comparison to the other two methods, the pressure centroid vortex tilt profiles were smoother and more coherent (Figs. 6a–c). The pressure centroid vortex tilt varied smoothly in magnitude and direction throughout the depth of the vortex at all three times shown, with the minor exception of the 6–8-km layer at 0200 UTC (Fig. 6a) where the vortex tilt abruptly shifted from northeast to west-northwest. The 0–8-km vortex tilt was persistently downshear left, consistent with previous modeling (e.g., Braun et al. 2006; Riemer et al. 2010) and observational (e.g., Nguyen and Molinari 2012; Reasor et al. 2013) studies of tropical cyclones in sheared environments. There was a distinct clockwise curvature with height of the vortex tilt, which was present throughout the 0000–1200 UTC period (not shown). Similar curvature of vortex tilt has been observed in airborne dual-Doppler radar analysis of intense tropical cyclones, both in case studies (e.g., Marks et al. 1992; Reasor and Eastin 2012) and in a composite mean of 75 TC flights in 19 tropical cyclones (Reasor et al. 2013). How often this curved vortex tilt occurs in simulations of tropical cyclones in shear and in nature, and what physical processes are responsible are not currently well known or well understood.

d. *Sensitivity to horizontal resolution*

To explore the impact of varying the horizontal grid resolution, each method was also tested using the 3-km domain output. Figure 7 shows the difference (in kilometers) between the analyzed TC center using 3-km domain output and the analyzed TC center using 1-km domain output for each of the four methods. The larger the difference, the more sensitive the method was to changes in the horizontal resolution of the data. The PV centroid method was quite sensitive to the change in horizontal resolution, with center differences between 10 and 30 km throughout the 12-h period. The maximum circulation center differences were more than 25 km at 0100, 0400, and 0600 UTC, but were smaller than 10 km at all other hourly times. The maximum tangential wind center differences were generally very small, except at 0400 UTC when the difference was near 20 km. The pressure centroid remained in nearly the same location throughout the 12-h period, regardless of whether 3- or 1-km domain data were used. This insensitivity suggests that the pressure centroid method would be effective for a range of high-resolution simulations.

The sensitivity of the PV centroid method to the horizontal resolution was likely due to the smoothing of intense, finescale PV maxima, reducing the magnitude of the PV maxima in the 3-km domain. This altered how the PV maxima were weighted in the PV centroid calculation [Eq. (1)], resulting in a shift of the PV centroid

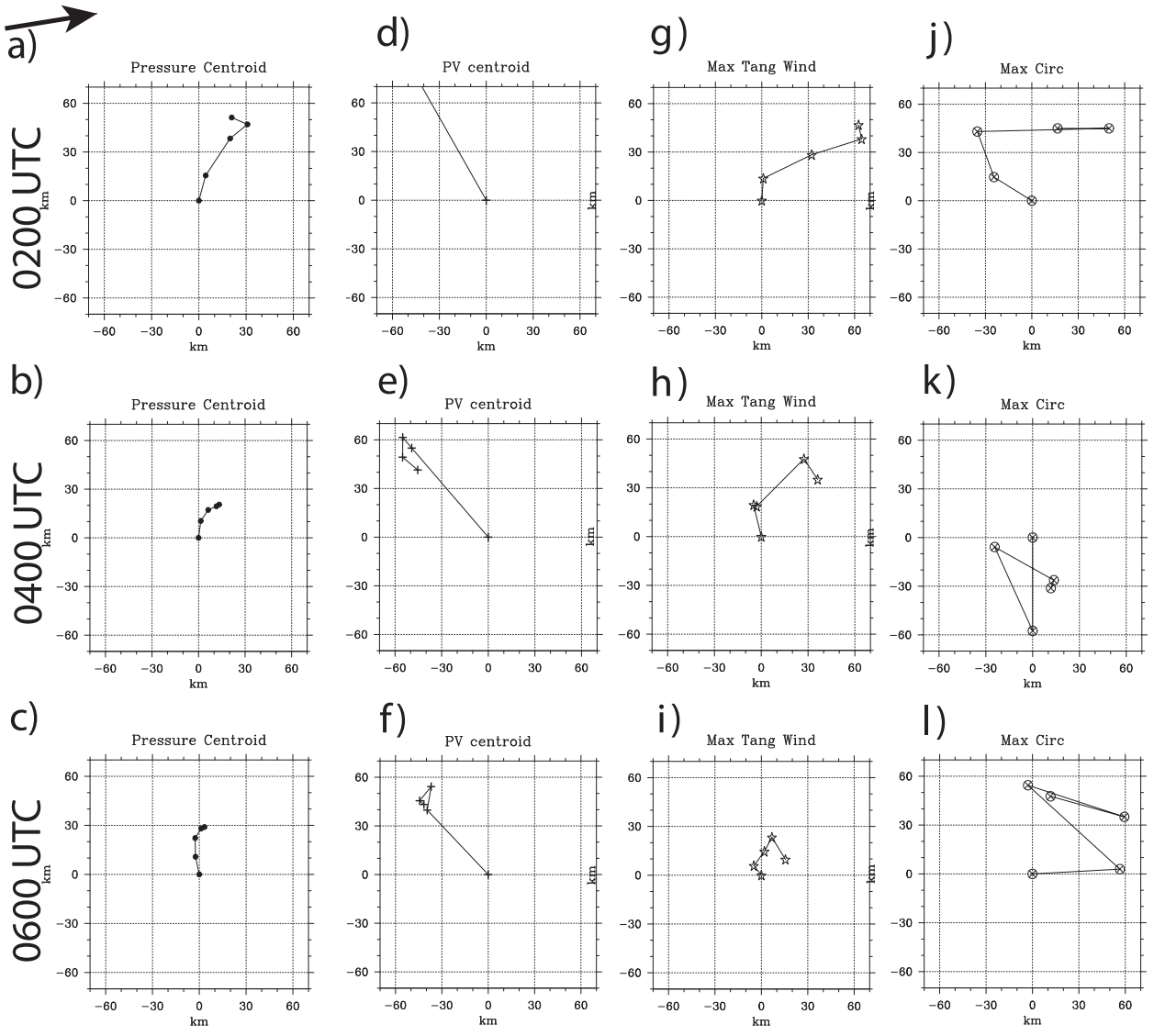

FIG. 6. Tropical cyclone vortex center positions at 2-km height intervals starting from the surface (shown at the origin) up to 8-km height. (a)–(c) The vortex tilt profile using the pressure centroid, (d)–(f) the potential vorticity method, (g)–(i) the maximum tangential wind method, and (j)–(l) the maximum circulation method. The pressure centroid, PV centroid, and maximum circulation methods used 100 km as the outer radius (see section 4). (top left) The approximate shear direction is shown.

slightly toward the region of weaker storm-relative winds. This smoothing effect is likely similar to what would occur in simulations using coarser resolution, because the magnitude of PV maxima tends to decrease with coarsening horizontal resolution in models (Gentry and Lackmann 2010). We speculate that the smoothing of intense, localized relative vorticity maxima played a role in the sensitivity of the maximum circulation method as well.

Although the maximum tangential wind center differences were generally very small, one notable exception occurred at 0400 UTC. Because the TC's tangential wind field was spatially broad early in the period, a large number of grid points had nearly equivalent maximum azimuthally averaged storm-relative tangential wind (not shown). As a result, very slight changes to the wind field due to coarsening the data resolution resulted in a substantial shift in the analyzed TC center position at 0400 UTC. This result suggests that the maximum tangential wind method could be more sensitive and perform inconsistently in TCs with a spatially broad tangential wind field.

The overall effectiveness of the pressure centroid can be attributed to the smoothing effect of the inverse Laplacian operator (Hoskins et al. 1985). Following quasi-geostrophic theory, both vorticity and potential vorticity

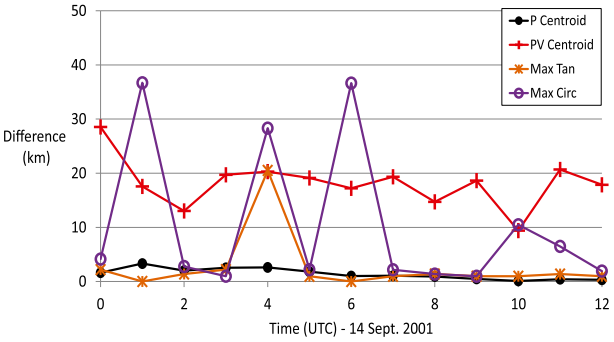

FIG. 7. The difference (km) between each method's 2-km height TC center location using the 1-km domain output vs using the 3-km domain output. The 0–100-km pressure centroid (black), 0–100-km potential vorticity centroid (red), maximum 100-km circulation (purple), and maximum tangential wind methods (orange) are shown.

contain the Laplacian of the pressure field. As a result, the small-scale high-amplitude convective features expressed in the vorticity and PV fields are smoothed over in the pressure field. This basic relationship also holds for the nonlinear balance approximation [see Eq. (11) in Raymond (1992)] that is more applicable for the tropical cyclone environment.

The PV centroid including the full PV field instead of just the positive PV was also tested for each of the above criteria. The full-PV centroid differed substantially in location from the positive-PV centroid (not shown), but the performance of the full-PV centroid did not differ meaningfully from the positive-PV centroid. As with the positive-PV centroid, the full-PV centroid was consistently displaced from the region of weakest storm-relative winds, yielded an erratic track, had an irregular, unrealistic vortex tilt, and was similarly sensitive to the change in horizontal data resolution.

e. Impact on physical interpretation

The differences among the TC center identification methods discussed above can lead to widely varying physical interpretations. One example is Fig. 8, which shows the 10-m storm-relative radial wind in each shear-relative quadrant using the four TC center identification methods. Note the large variability in the radial wind between the four methods, particularly at smaller radii where the radial wind is expected to be most sensitive to the TC center location. Numerous observational (e.g., Reasor et al. 2013) and modeling studies (e.g., Braun et al. 2006; Wu et al. 2006) have shown enhanced low-level inflow in the downshear quadrants and weakened inflow in the upshear quadrants. This azimuthal wavenumber-1 asymmetry in radial wind has been shown to be more pronounced in TCs within stronger ambient vertical wind shear. The pressure centroid, maximum tangential wind, and maximum circulation methods all reproduce this asymmetry. In contrast, the PV centroid method yields the strongest inflow in the upshear-right and downshear-right quadrants, and the weakest inflow in the upshear-left and downshear-left quadrants. This failure to reproduce the typical inflow asymmetry observed in sheared TCs could be erroneously interpreted as an anomalous TC response to the shear, if the discrepancies between TC center identification methods are not taken into account.

6. Sensitivity of the pressure centroid, PV centroid, and maximum circulation methods to the radius chosen

Recall that the outer radius (R) in Eqs. (1) and (2) represents the size of the tropical cyclone inner core, and that R was held fixed at 100 km in the previous section to facilitate comparison between center identification methods. However, the size of the TC inner core (and hence R) can vary greatly from storm to storm, and even within the same storm at different times. Also, the pressure centroid, PV centroid, and the maximum circulation center exhibit some sensitivity to the value of R. Figure 9 shows the pressure centroid, PV centroid, and the maximum circulation center using outer radii from 20 to 200 km in 20-km increments. Not surprisingly, when R = 20 km, both the pressure and PV centroids honed in on the mesovortex at 0200 (Fig. 9a) and 0400 UTC (Fig. 9b), while the maximum circulation center focused on the mesovortex only at 0400 UTC (Fig. 9b). This is because the pressure, PV, and relative vorticity anomalies associated with the mesovortex carry much more weight within such a small region. As R increased, the PV centroid and maximum circulation center shift generally toward the east and south, respectively, and into the region of stronger storm-relative winds. In contrast, the pressure centroid remained confined to the region of weak storm-relative winds. Note also in Fig. 9 that the black dots were spaced closer together than the red and white dots, indicating that the pressure centroid method was less sensitive to R than the PV centroid and maximum circulation methods. This provided additional evidence that the pressure centroid method performed better than the PV centroid and maximum circulation methods at identifying the TC center. Because the pressure centroid location varied with R, a method of selecting a value of R that reflects the size of the TC inner core was needed.

7. Selecting an optimum radius to calculate the pressure centroid

To account for the variability in tropical cyclone size, compositing studies have often normalized by the radius

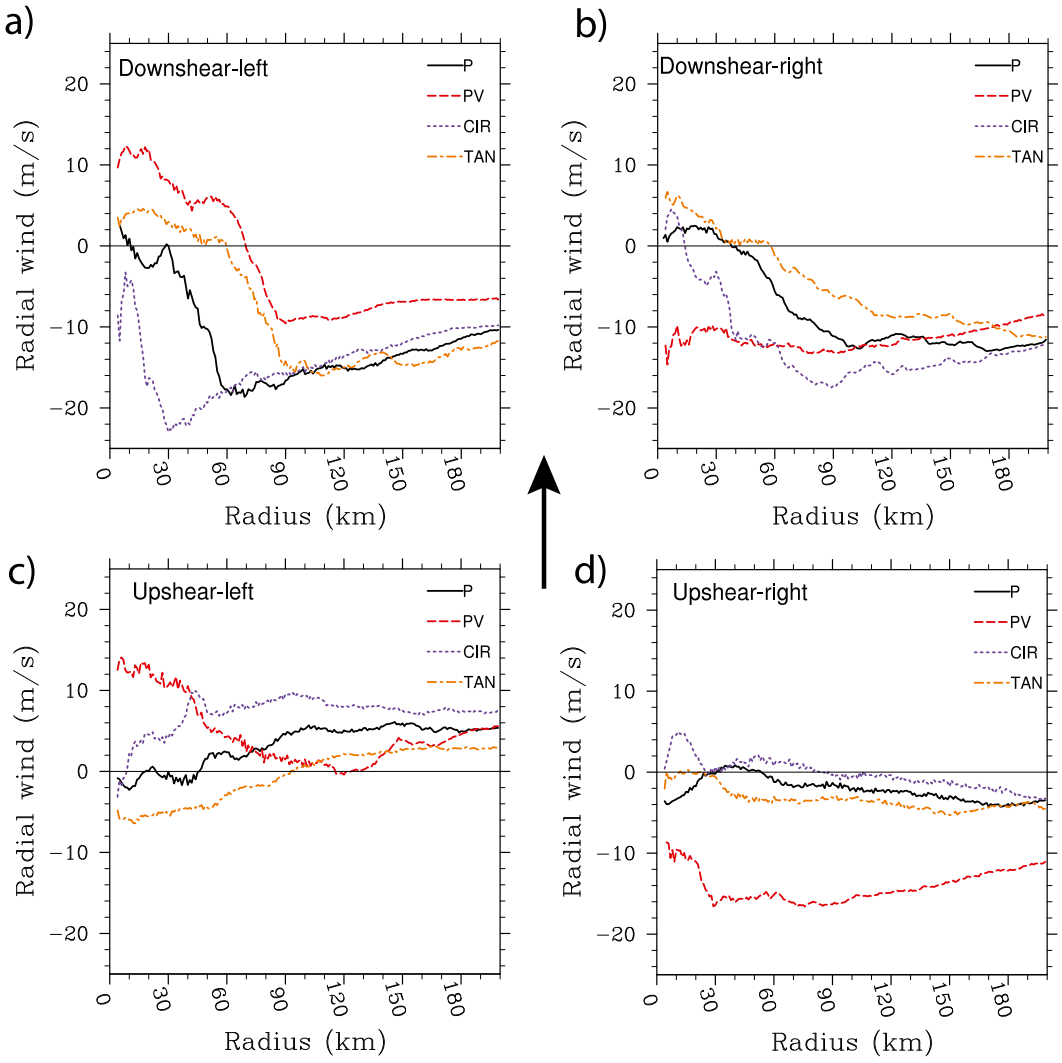

FIG. 8. Storm-relative 10-m radial wind in each shear-relative quadrant determined using the TC center from the 0–100-km pressure centroid (black), 0–100-km potential vorticity centroid (red), maximum 100-km circulation (purple), and maximum tangential wind (orange) methods. The shear vector points toward the top of the page.

of maximum wind (e.g., Rogers et al. 2012; Reasor et al. 2013), particularly in intense tropical cyclones with peaked tangential wind profiles. Figure 10a shows the azimuthally averaged storm-relative tangential wind at 2-km height early in the intensification period using the 0–100-km pressure centroid as the TC center. At this time, the tangential wind profile flattened beyond the 75-km radius. Although the RMW was analyzed at 125 km, just a small increase in the tangential wind at 170 km would shift the RMW to that radius. As discussed by Bell and Lee (2012), the RMW often exhibits large variability in tropical cyclones with flat tangential wind profiles, even when changes to the tangential wind profile are slight. In such cases, substantial shifts in the RMW are not reflective of substantial changes in TC size. This necessitates the use of an alternate normalization method that also performs effectively in TCs with relatively flat tangential wind profiles.

We propose normalizing by the innermost radius at which the azimuthally averaged storm-relative tangential wind at 2-km height equals P% of the maximum (R_P) at 2-km height, where P represents a subjectively chosen high percentage from 50 to 100. The 2-km height was chosen to be consistent with dual-Doppler radar studies, which typically composite data with respect to the RMW at 2-km height (e.g., Reasor et al. 2013). Figure 10b shows the time evolution of RMW, R_{90}, R_{80}, and R_{70}. The RMW experienced several large, abrupt shifts as well as many more high-frequency, lower-amplitude oscillations. Most notably, at about 0130 UTC,

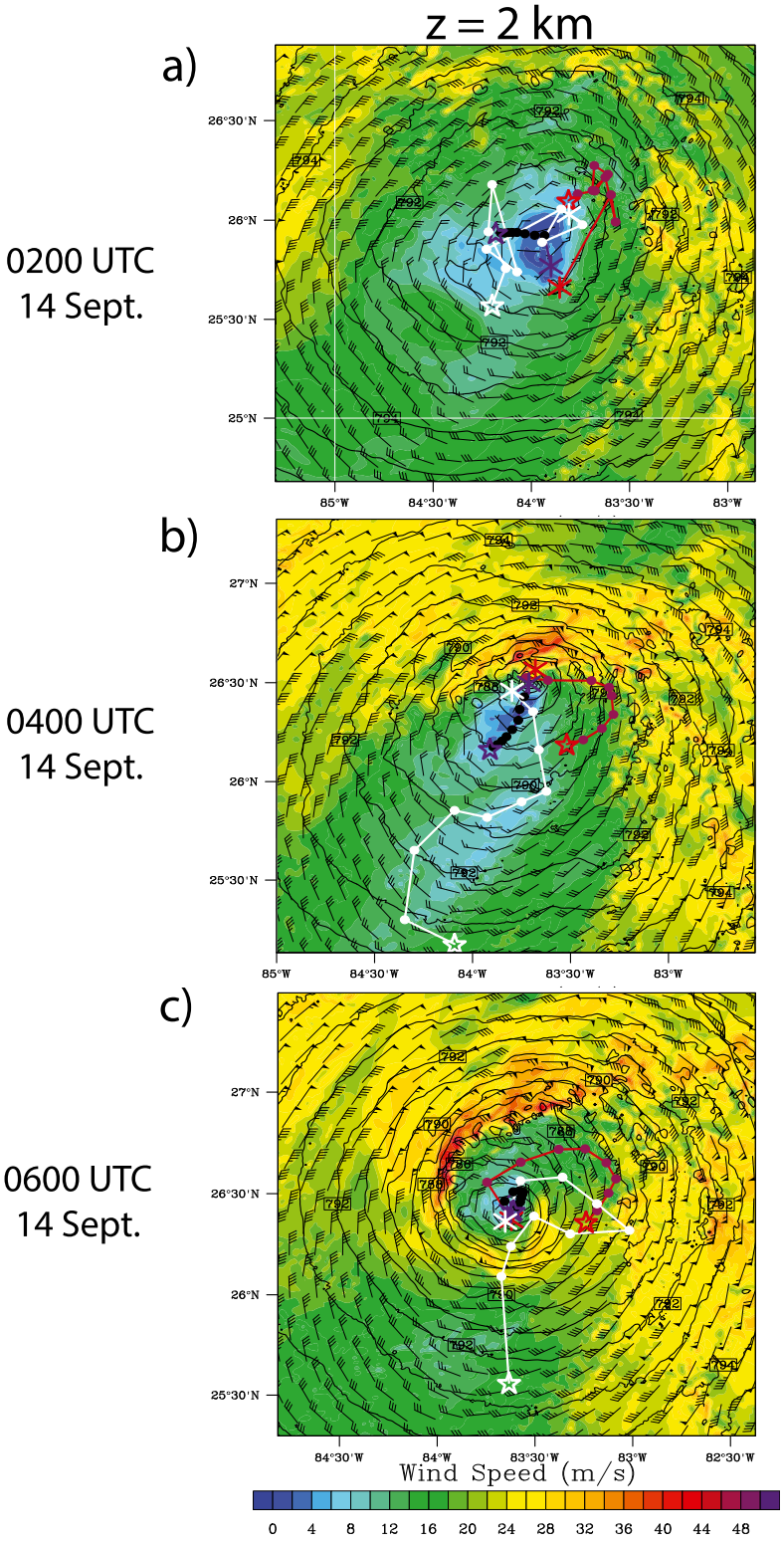

FIG. 9. As in Fig. 4, but only at 2-km height. The purple line denotes the pressure centroid location using varying outer radii from 20 km (asterisk symbol) in 20-km increments (black dots) out to 200 km (star symbol). The red line denotes the potential vorticity centroid. The white line denotes the maximum circulation center.

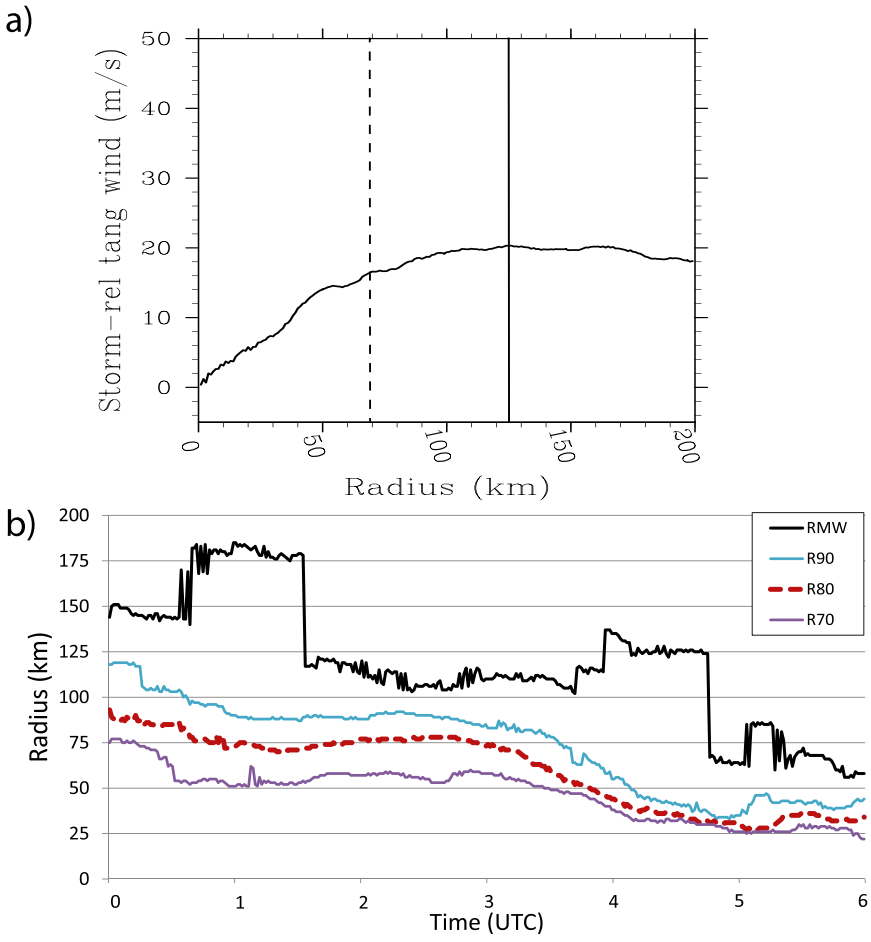

FIG. 10. (a) Azimuthally averaged storm-relative tangential wind at 0200 UTC 14 Sep. The solid vertical line shows the radius of maximum wind (RMW), while the dashed vertical line shows the innermost radius (R_{80}) at which the azimuthally averaged storm-relative tangential wind equals 80% of the maximum azimuthally averaged storm-relative tangential wind. (b) RMW (black), R_{90} (cyan), R_{80} (red), and R_{70} (purple) between 0000 and 0600 UTC 14 Sep.

the RMW abruptly jumped from 178 to 117 km, and at about 0445 UTC, the RMW jumped from 124 to 67 km. These shifts in the RMW were likely due to the sensitivity of the RMW to slight changes in the flat tangential wind profile, and did not accurately reflect changes in the size of the TC. In contrast, R_{90}, R_{80}, and R_{70} all varied much more smoothly with time, indicating that they were less sensitive to small changes in the flat tangential wind profile. This suggests that normalizing by R_{90}, R_{80}, or R_{70} is more effective than normalizing by the RMW.

To choose the optimal percentage for P, two factors must be taken into consideration. First, P should not be too close to 100, because R_P approaches the RMW as P approaches 100. On the other hand, as P decreases, R_P is increasingly influenced by whether the tangential wind profile is U shaped or V shaped inside the RMW (e.g., Kossin and Eastin 2001; Wood et al. 2013) as opposed to changes in the TC size. Taking both of these factors into consideration, we subjectively choose $P = 80$ as the optimal percentage in this paper. Note in Fig. 10a that even if the tangential wind at 170 km increased slightly and the RMW moved to that radius, R_{80} would shift outward only very slightly. Because the circle with radius R_{80} does not capture the entire inner core of the tropical cyclone vortex, we propose using $2R_{80}$ as the measure of TC inner core size in Eq. (2). The pressure centroids calculated using a circle of radius $2R_{80}$ performed well according to the criteria introduced in section 5 (not shown).

To summarize, the recommended procedure to calculate the tropical cyclone center is as follows: use Eq. (2) with the pressure minimum location as the initial TC center and $R = 100$ km as a first guess to calculate a first-guess pressure centroid. Then, from the resulting azimuthally averaged tangential wind profile at 2-km height, calculate the value of R_{80}, and use $2R_{80}$ as the

value for R in Eq. (2) to calculate the next-guess pressure centroid. Finally, iterate until the pressure centroid settles onto a single location.

8. Discussion

A 1-km horizontal resolution WRF simulation of a sheared, intensifying tropical cyclone was performed. A strong mesovortex and other convective asymmetries that developed made this an ideal and challenging case to assess and compare several tropical cyclone center identification methods. The center positions proved to be very sensitive to the TC center identification method used. The performance of these methods was assessed based on four criteria: 1) the TC center should be located within the region of weak storm-relative wind, 2) the motion of the TC center should be smooth over time and should not abruptly change speed and/or direction on an hourly time scale, 3) the vortex tilt should vary smoothly in magnitude and direction throughout the depth of the vortex, and 4) simply changing the horizontal resolution of the model output should not have a significant impact on the analyzed TC center location. By all four metrics, the pressure centroid method consistently outperformed the other center identification methods. This can be attributed to the smoothing effect of the inverse Laplacian operator (Hoskins et al. 1985). Because the vorticity and potential vorticity contain the Laplacian of the pressure field, the localized high-amplitude convective features in the vorticity and potential vorticity field were smoothed over in the pressure field. This smoothing effect also has implications for the broader applicability of each of the center identification methods. Because the pressure field was smoother, the pressure centroid method was less affected by changes in the horizontal resolution of the data. This suggests that the pressure centroid method would remain the most effective method in simulations of different horizontal resolutions.

The pressure centroid was calculated within a circle of radius R [Eq. (2)], which represents the TC inner core. Because the pressure centroid exhibited sensitivity to R, a procedure was needed to select an R that captured the TC inner core size. Although compositing studies have often normalized by the radius of maximum wind to account for varying TC size, this method is less effective in TCs with flat tangential wind profiles. Instead, we propose normalizing by R_{80}, the radius at which the azimuthally averaged storm-relative tangential wind at 2-km height is equal to 80% of the maximum at 2-km height. Here R_{80} was less sensitive to small changes in flat tangential wind profiles than the RMW. Both R_{70} and R_{90} were also tested and were similarly insensitive. Since the circle with radius R_{80} is smaller than the TC inner core, we propose using $2R_{80}$ as the measure of TC inner core size in Eq. (2). The aforementioned normalization technique can also be used to composite modeling output or observational data within TCs that have relatively flat tangential wind profiles, when the RMW normalization technique is ineffective.

It should be noted that there are limitations with the pressure centroid method. Because the method requires a contiguous region of pressures lower than the environmental pressure, the pressure centroid method should not be used with any pre-TC disturbance that does not contain a closed isobar (i.e., easterly waves or troughs of low pressure). Also, the use of the pressure centroid requires knowledge of the full pressure field. Because of the poor spatiotemporal coverage of aircraft and other observational data platforms, the pressure centroid method can only be applied to numerical models.

The considerable sensitivity of center position estimates and vortex tilt profiles to TC center identification methods illustrates the attention that needs to be paid to the center identification method used. This is especially true in cases when TC center identification is less straightforward, such as in high-resolution simulations of weaker TCs, asymmetric TCs, and TCs with broad tangential wind fields. Based on the results presented here, we recommend using the pressure centroid to define the tropical cyclone center in high-resolution numerical models, as it holds promise for identifying a physically consistent and meaningful center for TCs of varying structures and intensities.

Acknowledgments. We thank Ryan Torn of our department for his suggestions regarding the model setup and choice of model physics. We thank two anonymous reviewers for their insightful and constructive comments that improved the quality of this manuscript. This work was supported by NSF Grant ATM AGS1132576.

REFERENCES

Bell, M. M., and W. Lee, 2012: Objective tropical cyclone center tracking using single-Doppler radar. *J. Appl. Meteor. Climatol.,* **51,** 878–896, doi:10.1175/JAMC-D-11-0167.1.

Braun, S. A., 2002: A cloud-resolving simulation of Hurricane Bob (1991): Storm structure and eyewall buoyancy. *Mon. Wea. Rev.,* **130,** 1573–1592, doi:10.1175/1520-0493(2002)130<1573:ACRSOH>2.0.CO;2.

——, M. T. Montgomery, and Z. Pu, 2006: High-resolution simulation of Hurricane Bonnie (1998). Part I: The organization of eyewall vertical motion. *J. Atmos. Sci.,* **63,** 19–42, doi:10.1175/JAS3598.1.

Cavallo, S. M., R. D. Torn, C. Snyder, C. Davis, W. Wang, and J. Done, 2013: Evaluation of the Advanced Hurricane WRF Data Assimilation System for the 2009 Atlantic hurricane

season. *Mon. Wea. Rev.,* **141,** 523–541, doi:10.1175/MWR-D-12-00139.1.

Dudhia, J., 1989: Numerical study of convection observed during the winter monsoon experiment using a mesoscale two-dimensional model. *J. Atmos. Sci.,* **46,** 3077–3107, doi:10.1175/1520-0469(1989)046<3077:NSOCOD>2.0.CO;2.

Gentry, M. S., and G. M. Lackmann, 2010: Sensitivity of simulated tropical cyclone structure and intensity to horizontal resolution. *Mon. Wea. Rev.,* **138,** 688–704, doi:10.1175/2009MWR2976.1.

Griffin, J. S., R. W. Burpee, F. D. Marks, and J. L. Franklin, 1992: Real-time airborne analysis of aircraft data supporting operational hurricane forecasting. *Wea. Forecasting,* **7,** 480–490, doi:10.1175/1520-0434(1992)007<0480:RTAAOA>2.0.CO;2.

Hong, Y.-Y., and J.-O. J. Lim, 2006: The WRF single-moment 6-class microphysics scheme (WSM6). *J. Korean Meteor. Soc.,* **42,** 129–151.

Hoskins, B. J., M. E. McIntyre, and A. W. Robertson, 1985: On the use and significance of isentropic potential vorticity maps. *Quart. J. Roy. Meteor. Soc.,* **111,** 877–946, doi:10.1002/qj.49711147002.

Jordan, C. L., 1966: Surface pressure variations at coastal stations during the period of irregular motion of Hurricane Carla of 1961. *Mon. Wea. Rev.,* **94,** 454–458, doi:10.1175/1520-0493(1966)094<0454:SPVACS>2.3.CO;2.

Kain, J. S., and J. M. Fritsch, 1993: Convective parameterization for mesoscale models: The Kain–Fritcsh scheme. *The Representation of Cumulus Convection in Numerical Models, Meteor. Monogr.,* No. 46, Amer. Meteor. Soc., 165–170.

Kossin, J. P., and M. D. Eastin, 2001: Two distinct regimes in the kinematic and thermodynamic structure of the hurricane eye and eyewall. *J. Atmos. Sci.,* **58,** 1079–1090, doi:10.1175/1520-0469(2001)058<1079:TDRITK>2.0.CO;2.

Lee, W., and F. D. Marks, 2000: Tropical cyclone kinematic structure retrieved from single-Doppler radar observations. Part II: The GBVTD-simplex center finding algorithm. *Mon. Wea. Rev.,* **128,** 1925–1936, doi:10.1175/1520-0493(2000)128<1925:TCKSRF>2.0.CO;2.

Liu, Y., D.-L. Zhang, and M. K. Yau, 1999: A multiscale numerical study of Hurricane Andrew (1992). Part II: Kinematics and inner-core structures. *Mon. Wea. Rev.,* **127,** 2597–2616, doi:10.1175/1520-0493(1999)127<2597:AMNSOH>2.0.CO;2.

Marks, F. D., R. A. Houze, and J. F. Gamache, 1992: Dual-aircraft investigation of the inner core of Hurricane Norbert. Part I: Kinematic structure. *J. Atmos. Sci.,* **49,** 919–942, doi:10.1175/1520-0469(1992)049<0919:DAIOTI>2.0.CO;2.

Mlawer, E. J., S. J. Taubman, P. D. Brown, M. J. Iacono, and S. A. Clough, 1997: Radiative transfer for inhomogeneous atmospheres: RRTM, a validated correlated-k model for the longwave. *J. Geophys. Res.,* **102,** 16 663–16 682, doi:10.1029/97JD00237.

Molinari, J., and D. Vollaro, 2010: Rapid intensification of a sheared tropical storm. *Mon. Wea. Rev.,* **138,** 3869–3885, doi:10.1175/2010MWR3378.1.

——, P. Dodge, D. Vollaro, K. L. Corbosiero, and F. Marks, 2006: Mesoscale aspects of the downshear reformation of a tropical cyclone. *J. Atmos. Sci.,* **63,** 341–354, doi:10.1175/JAS3591.1.

Montgomery, M. T., M. E. Nicholls, T. A. Cram, and A. B. Saunders, 2006: A vortical hot tower route to tropical cyclogenesis. *J. Atmos. Sci.,* **63,** 355–386, doi:10.1175/JAS3604.1.

Murillo, S. T., W. Lee, M. M. Bell, G. M. Barnes, F. D. Marks, and P. P. Dodge, 2011: Intercomparison of Ground-Based Velocity Track Display (GBVTD)-retrieved circulation centers and structures of Hurricane Danny (1997) from two coastal WSR-88Ds. *Mon. Wea. Rev.,* **139,** 153–174, doi:10.1175/2010MWR3036.1.

Nguyen, L. T., and J. Molinari, 2012: Rapid intensification of a sheared, fast-moving hurricane over the Gulf Stream. *Mon. Wea. Rev.,* **140,** 3361–3378, doi:10.1175/MWR-D-11-00293.1.

Noh, Y., W. G. Cheon, S. Y. Hong, and S. Raasch, 2003: Improvement of the K-profile model for the planetary boundary layer based on large eddy simulation data. *Bound.-Layer Meteor.,* **107,** 401–427, doi:10.1023/A:1022146015946.

Raymond, D. J., 1992: Nonlinear balance and potential-vorticity thinking at large Rossby number. *Quart. J. Roy. Meteor. Soc.,* **118,** 987–1015, doi:10.1002/qj.49711850708.

Reasor, P. D., and M. T. Montgomery, 2001: Three-dimensional alignment and corotation of weak, TC-like vortices via linear vortex Rossby waves. *J. Atmos. Sci.,* **58,** 2306–2330, doi:10.1175/1520-0469(2001)058<2306:TDAACO>2.0.CO;2.

——, and M. D. Eastin, 2012: Rapidly intensifying Hurricane Guillermo (1997). Part II: Resilience in shear. *Mon. Wea. Rev.,* **140,** 425–444, doi:10.1175/MWR-D-11-00080.1.

——, R. Rogers, and S. Lorsolo, 2013: Environmental flow impacts on tropical cyclone structure diagnosed from airborne Doppler radar composites. *Mon. Wea. Rev.,* **141,** 2949–2969, doi:10.1175/MWR-D-12-00334.1.

Riemer, M., M. T. Montgomery, and M. E. Nicholls, 2010: A new paradigm for intensity modification of tropical cyclones: Thermodynamic impact of vertical wind shear on the inflow layer. *Atmos. Chem. Phys.,* **10,** 3163–3188, doi:10.5194/acp-10-3163-2010.

Rogers, R., S. Lorsolo, P. Reasor, J. Gamache, and F. Marks, 2012: Multiscale analysis of tropical cyclone kinematic structure from airborne Doppler radar composites. *Mon. Wea. Rev.,* **140,** 77–99, doi:10.1175/MWR-D-10-05075.1.

Skamarock, W. C., and Coauthors, 2008: A description of the Advanced Research WRF version 3. NCAR Tech. Note NCAR/TN-475+STR, 113 pp. [Available online at http://www.mmm.ucar.edu/wrf/users/docs/arw_v3_bw.pdf.]

Willoughby, H. E., 1992: Linear motion of a shallow-water barotropic vortex as an initial-value problem. *J. Atmos. Sci.,* **49,** 2015–2031.

——, and M. B. Chelmow, 1982: Objective determination of hurricane tracks from aircraft observations. *Mon. Wea. Rev.,* **110,** 1298–1305, doi:10.1175/1520-0493(1982)110<1298:ODOHTF>2.0.CO;2.

Wood, V. T., L. W. White, H. E. Willoughby, and D. P. Jorgensen, 2013: A new parametric tropical cyclone tangential wind profile model. *Mon. Wea. Rev.,* **141,** 1884–1909, doi:10.1175/MWR-D-12-00115.1.

Wu, L., S. A. Braun, J. Halverson, and G. Heymsfield, 2006: A numerical study of Hurricane Erin (2001). Part I: Model verification and storm evolution. *J. Atmos. Sci.,* **63,** 65–86, doi:10.1175/JAS3597.1.